9 Application of Computational Fluid Dynamics Methods to Understand Nasal Cavity Flows

Andreas Lintermann

In recent years, computational fluid dynamics (CFD) methods have become a valuable tool to analyze the intricate flow in the human nasal cavity. Early studies addressed the flow in artificial models of the nasal cavity [1–5]. The availability of high-resolution computed tomography (CT) or magnetic resonance tomography (MRT) data and the corresponding software to pre-process medical images enabled, however, to investigate realistic and individual nasal cavity geometries by means of numerical simulations [6–20]. To exploit the capabilities of CFD methods to predict nasal cavity flows, an overview of different approaches that are frequently used in the field of respiratory-related bio-fluid mechanics is given in this chapter. In more detail, Sect. 9.1 presents a general approach to pre-process medical data for flow simulations. Subsequently, meshing methods for space discretization are discussed in Sect. 9.2 before an overview of different simulation methods is given in Sect. 9.3. In Sect. 9.4, tools for the analysis of the flow in the human nasal cavity as computed by CFD methods are discussed and finally, in Sect. 9.5, potentials to use such methods in clinical applications are highlighted.

9.1 Pre-Processing Medical Image Data for the Use in Numerical Simulations

The preparation of medical image data for CFD-based analyses usually follows a certain pipeline [15, 21]. Starting from the acquired CT or MRT data, the surface of the nasal cavity is extracted from these images either by the support of radiologists and ENT specialists using manual segmentation or by (semi-)automatic segmentation tools. The segmentation method basically depends on the quality and type of the available image data. That is, in case of MRT data, tissue and air is often difficult to distinguish and the resolution is often quite low. Hence, experienced personnel need to identify the volume of interest, i.e., the air volume within the nasal cavity. In contrast, CT images feature hard interfaces between air and tissue. They can be identified by strong gradients in the Hounsfield data by automatic segmentation algorithms. From the extracted air volume, nasal cavity surfaces are generated via a 3D reconstruction algorithm [22]. The resulting surfaces are discrete approximations to the real nasal cavity and often require to apply non-shrinking smoothing algorithms [23] to remove stair-step artifacts originating from the discrete voxel-structure of the medical images. In the end of this pre-processing step, such surfaces are often given by a collection of triangles that in sum define a watertight two-manifold surface. Tools that are frequently used for pre-processing are, amongst others, 3D Slicer[1] [24], the Medical Imaging Interaction Toolkit (MITK)[2] [25], OsiriX[3] [26], or software packages from Materialise.[4]

9.2 Space-Discretization through Meshing

The equations describing the physics of fluid flow, which are solved in numerical simulations are either given in integral or in partial derivative form. Computers, however, require the equations to be in their discrete formulation, i.e., integrals and derivatives need to be approximated by their according discrete form. To account for the discretization of the equations and to find numerical solutions, the space is split into small

The original version of this chapter was revised. A correction to this chapter can be found at https://doi.org/10.1007/978-3-030-21217-9_106

A. Lintermann (✉)
Institute of Aerodynamics and Chair of Fluid Mechanics, RWTH Aachen University, Aachen, Germany

Simulation Laboratory Highly Scalable Fluids and Solids Engineering, Jülich Aachen Research Alliance Center for Simulation and Data Science (JARA-CSD), RWTH Aachen University, Aachen, Germany
e-mail: a.lintermann@aia.rwth-aachen.de

[1] 3D Slicer https://www.slicer.org
[2] MITK http://mitk.org
[3] OsiriX http://osirix-viewer.com
[4] Materialise http://biomedical.materialise.com

C. Cingi, N. Bayar Muluk (eds.), *All Around the Nose*, https://doi.org/10.1007/978-3-030-21217-9_9

discrete volumes. This procedure is called meshing or grid generation and delivers the volume of interest partitioned into small volumetric elements, which in sum constitute the computational grid. Depending on the simulation method, such grids may consist of a collection of tetrahedrals or prisms, a combination of both that smoothly adapt to the surface of the nasal cavity, or of a collection of cubes that may stick out of the surface and that require a second pre-processing before a simulation can be run. The discrete elements are also referred to as computational cells and will in the simulation contain information on the flow such as the pressure, temperature, velocity, or density. Computational meshes can be structured or unstructured. That is, structured meshes allow for a continuous cell indexing (i, j, k) for all three space dimensions, where the neighborhood of a cell is uniquely identifiable by $(i \pm 1, j \pm 1, k \pm 1)$. Simulation codes using structured meshes are in general fast due to aligned memory access, however, necessitate to construct the meshes manually for complex shapes. This makes them rather unsuitable for the simulation of nasal cavity flows. In contrast, memory access in unstructured meshes like tetrahedral, hybrid tetrahedral/prism, and Cartesian meshes (cube meshes) is less efficient due to the non-continuous indexing. However, such meshes can be constructed fully automatically, especially the generation of hierarchical Cartesian meshes that define in 3D an octree structure by parent–child relationships between coarse cells and finer cells can be implemented very efficiently [27]. The parent-child relationship in such meshes is obatined by continous subdivision of the cells in the octree. In all meshing cases, the volume or the spatial distance of these cells defines the resolution of the mesh and hence it also determines the quality of the simulation output. While laminar flow requires in general low resolutions, high Reynolds-number flows, i.e., cases where the inertial forces are way bigger than the viscous forces, transitional and turbulent flow appears, and high gradients of the flow variables are expected, high mesh resolutions are required to resolve all flow features. Mathematically, the Reynolds number is defined by $Re = u \cdot D/v$, where u is a reference velocity, D is some characteristic length, and v is the kinematic viscosity of the fluid. Furthermore, the force acting on the tissue in addition to the pressure, namely, the wall-shear stress, is frequently of interest. Its computation requires an accurate evaluation of the velocity gradient close to the wall. Therefore, the boundary layer, whose thickness is a function of the Reynolds number, needs to be resolved by refined meshes close to the wall to obtain an accurate representation of the gradient. Examples of different mesh types are depicted in Fig. 9.1

To show that the resolution of a mesh is sufficient, so-called grid dependence studies are usually performed. Therefore, the same simulation is run at different resolutions and the results are juxtaped. That is, the best resolution is determined, e.g., by comparing local flow profiles, general properties such as the pressure loss along a nasal cavity or the corresponding heating capability, by analyzing the accuracy of wall-shear stress computations or the flow field energy spectra. Latter delivers information on the range of structures that can be captured with a given resolution. Meshing tools can be categorized in commercially available, open source tools, and in-house methods. Some frequently used commercial tools are ANSYS ICEM CFD,[5] ANSYS Meshing,[6] PointwiseGridgen,[7] or SALOME,[8] which may provide various mesh types. Furthermore, the mesher in OpenFOAM,[9] snappyHexMesh,[10] and NETGEN[11] are freely available. In-house flow solvers sometimes also use their own meshing tools [27] that are suited for specific classes of problems and solution methods, allow for an automatization of the grid generation process, and are highly flexible when it comes to meshing of complex geometries.

9.3 Numerical Approaches to Solve the Governing Equations of Fluid Mechanics

In CFD simulations, the fundamental equations of motion, i.e., the conservation of mass, momentum, and energy (the Navier–Stokes equations) can be solved by numerous numerical schemes. Among the most popular ones are the finite volume (FV), finite element (FE), finite difference (FD), discontinuous Galerkin (DG), and the lattice-Boltzmann (LB) methods. Different sets of equations may be solved in this context, however, all of them can be derived from the Navier–Stokes equations. To be more specific, the Reynolds-averaged Navier–Stokes (RANS) equations, the Navier–Stokes equations with or without small-scale modeling approaches, or the Boltzmann equation are solved. Simulations solving the RANS equations are mainly suited for high-Reynolds-number flows. In this approach, the temporally averaged equations are solved and the flow is split into a mean and a fluctuating part. The derivation of the RANS equations leads to a new term, i.e., the Reynolds stresses that are required to be approximated by turbulence models. One can imagine this kind of method as running an under-resolved simulation delivering a mean flow and adding a model representing the energy transfer between small-

[5] ANSYS ICEM CFD http://resource.ansys.com/Products/Other+Products/ANSYS+ICEM+CFD

[6] ANSYS Meshing http://www.ansys.com/Products/Platform/ANSYS-Meshing

[7] PointwiseGridgen http://www.pointwise.com/pw

[8] SALOME http://www.salome-platform.org

[9] OpenFOAM http://www.openfoam.com

[10] snappyHexMesh https://github.com/nogenmyr/swiftSnap

[11] NETGEN http://www.hpfem.jku.at/netgen/

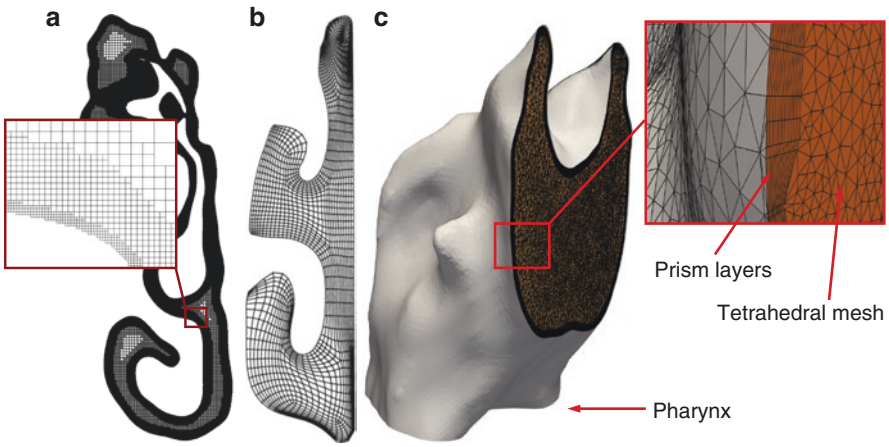

Fig. 9.1 Examples of different computational meshes used for CFD simulations in the human respiratory tract. (**a**) Cartesian mesh as constructed by a parallel grid generator [27]. (**b**) Manually generated block-structured mesh [2]. (**c**) Mixed tetrahedra/prism mesh

scale and continuously decaying structures. The approximations that are frequently used in RANS computations, e.g., the two equation-models k-ε [28] or k-ω [29], which deliver additional equations for the turbulent kinetic energy k and the dissipation ε or the vorticity ω, are derived for cases that have little in common with the intricate flow in the human respiratory tract. Furthermore, these models require empirical constants that need to be specifically tuned for the individual simulation case. Despite these drawbacks, RANS computations are often used in the community and in industry due to their attractive low computational costs. Another approach is running a large-eddy simulation (LES), which solves the spatially filtered Navier–Stokes equations and models the filtered parts by so-called sub-grid scale models. That is, models mimic the filtered fine-scale structures. LES computations allow for the simulation of temporally resolved flow fields that cover a larger range of turbulent structures than those covered by RANS computations. The method that does not model any scales at all is called a direct numerical simulation (DNS) in which the full Navier–Stokes equations are solved directly. DNS are the most expensive simulations. In contrast to RANS or LES computations they allow, however, for a fully detailed analysis of complex fluid flows.

FV methods solve the Navier–Stokes equations in their integral formulation, while FD methods use the partial differential formulation. FE methods and DG methods alike solve the problem by considering weak formulations of the Navier-Stokes equations. The LB method differs from all of the aforementioned approaches as it solves the discrete Boltzmann equation that describes the fate of gas particles by probability distribution functions and hence by statistical means. In LB methods, the macroscopic variables such as pressure, temperature, velocity, or density, can simply be obtained from the moments of these probability distribution functions, while in the other methods these variables are direct results of a simulation or need to be computed in addition. For example, in incompressible flows it is often required to solve the pressure-Poisson equation to obtain the pressure. Using these different methods, also the time is discretized. Marching foward in time, the next time step is either only dependent on the previous time step (explicit schemes) or on the previous and current time step (implicit schemes). In general, implicit schemes require to solve a huge linear system of equations and the time step is variable, while in explicit schemes the time step is fixed and the new state of the flow field can simply be determined from the last solution step. The interested reader is referred to [30] for FD and FV methods. A detailed description of LB methods can be found in [31] and the DG method is described in [32].

As previously mentioned, RANS computations are rather inexpensive and can be run in a short amount of time on smaller desktop machines. Unlike RANS simulations, LES and DNS computations require high processing power and a higher amount of available memory, i.e., desktop machines are too small to solve these problems in a reasonable amount of time. That is, such computations can only be performed on high-performance computers (HPC) that, nowadays in the petascale era, consist of hundreds of thousands of processing cores, each equipped with a certain amount of memory that sums up to several terabytes for the whole machine. For the simulation, the problem is distributed among the available processors such that each processor simulates only a small fraction of the whole problem. Obviously, each processor cannot solve the problem independently and hence information needs to be exchanged among the processors. This is realized by performing communication over the network across computational nodes. Fortunately, HPC networks are

designed for high communication throughput. On node-level, information exchange is either implemented by shared memory access or by direct communication between the participating CPU cores. Although current HPC systems use high-bandwidth and low-latency networks, indeed communication is one of the major issues that slows down simulation software and limits scaling across an extremely large number of computational cores. Algorithmic and hardware performance is hence an active field of research that guides software and HPC into the next generation supercomputing era (exascale era). Note that current HPC systems are mainly available for research institutes conducting large-scale simulations, however, as time evolves and computing power becomes more and more affordable, it will be possible to run LES computations on local cluster systems in the near future. Software that is frequently employed for the simulation of flows are either commercial tools like ANSYS Fluent,[12] ANSYS CFX,[13] CD-adapco products (STAR-CD,[14] STAR-CCM+[15]), EXA PowerFLOW,[16] open source codes like OpenFOAM, OpenLB,[17] Code Saturne,[18] or in-house codes like ZFS[19]and Alya,[20] developed at the Institute of Aerodynamics and Chair of Fluid Mechanics, RWTH Aachen University, and the Barcelona Supercomputing Center, respectively.

All of the aforementioned methods find application in the simulation of nasal cavity flows and have their advantages and disadvantages. However, to not distract the reader from the real problem, i.e., the simulation of nasal cavity flows, in the next section the focus is rather on the tools to analyze and understand the physics of the flow than on the applied method.

9.4 CFD Computations of the Flow in the Human Nasal Cavity

The most important aspect that determines the comfort of a patient is how easy it is to breathe. Swollen turbinates, perforated or bend septa lead to a reduced breathing capability, make respiration strenuous, and hence reduce the comfort of a patient. Considering inspiration, the facility to breath can simply be characterized by the amount of energy that is lost in the respiration process, i.e., the higher the energy loss the more difficult it is to inhalte. As already stated in Sect. 9.2, the energy required to inhale can be described by considering the pressure loss, i.e., by considering Bernoulli's equation [33]. However, one needs to take care that Bernoulli's equation is only valid along a streamline in steady, incompressible, and inviscid flow and that the outcome of such an analysis is hence only an approximation to the real pressure loss. Furthermore, it is important to note that Bernoulli's equation considers the total pressure, which consists of the static pressure and the dynamic pressure. Latter is basically the kinetic energy contribution of the moving fluid. This is unfortunately often omitted when analyzing the flow and only the static pressure difference is assumed to represent the pressure loss. Despite the fact that the share of the dynamic pressure is in general small, locally it may vary extremely due to fluid accelerations. For example, consider a flow without losses that passes an orifice, say an airway restriction in the nasal cavity. Then, Bernoulli's equation states that the total pressure is the same at the entry of the diverging part as at the orifice. Since the velocity increases due to the channel divergence, the dynamic pressure increases as well. This goes along with a decrease of the static pressure leading to the same values of the total pressure at both locations at the end. Streamlines in transient or quasi-steady simulations may rapidly change their course and are hence not very suited for the pressure loss evaluation. Hence, it either makes sense to consider the area-averaged total pressure difference of the nostrils and the pharynx or to place streamlines into the flow field that pass the regions to analyze and are based on time-averaged solutions. This is for example done in [9, 15, 34]. This way, one can obtain an integral pressure or energy loss using former method while with the latter localized information can be obtained that takes into account the local static and dynamic pressure. Plotting the accumulated loss along a streamline then delivers an idea where most of the energy is lost. An example of a streamline extracted from an averaged flow field is shown in Fig. 9.2a. The plot $\Delta p_{t,l}(N_m,s)$ in Figure 9.2b shows the accumulated total pressure loss along this streamline. Prominent locations for increased pressure loss are airway restrictions as they appear in the nasal valve or in swollen turbinates. Strong shear stress acting on the fluid that appears, e.g., in regions with high velocity gradients in wall-normal direction, at sharp corners, which may lead to flow separation, or in higher Reynolds number flows, are also important factors radically influencing the energy loss. It is hence not surprising that the pressure loss has been used widely [5, 9, 10, 15, 16, 19, 34, 35] to analyze the performance of nasal cavities. Especially, results of the ratio of the loss to the mass flux, or in other words, the Reynolds number, are helpful [5, 35] and can be compared to real rhinomanometry measurements [36]

[12] ANSYS Fluent http://www.ansys.com/Products/Fluids/ANSYS-Fluent

[13] ANSYS CFX http://www.ansys.com/Products/Fluids/ANSYS-CFX

[14] CD-adapco STAR-CD http://www.cd-adapco.com/products/star-cd

[15] CD-adapco STAR-CCM+ http://www.cd-adapco.com/products/star-ccm

[16] EXA PowerFLOW http://exa.com/product/simulation-tools/powerflow-cfd-simulation

[17] OpenLB http://optilb.org/openlb

[18] Code Saturne http://code-saturne.org

[19] ZFS http://www.aia.rwth-aachen.de

[20] Alya http://www.bsc.es/es/computer-applications/alya-system

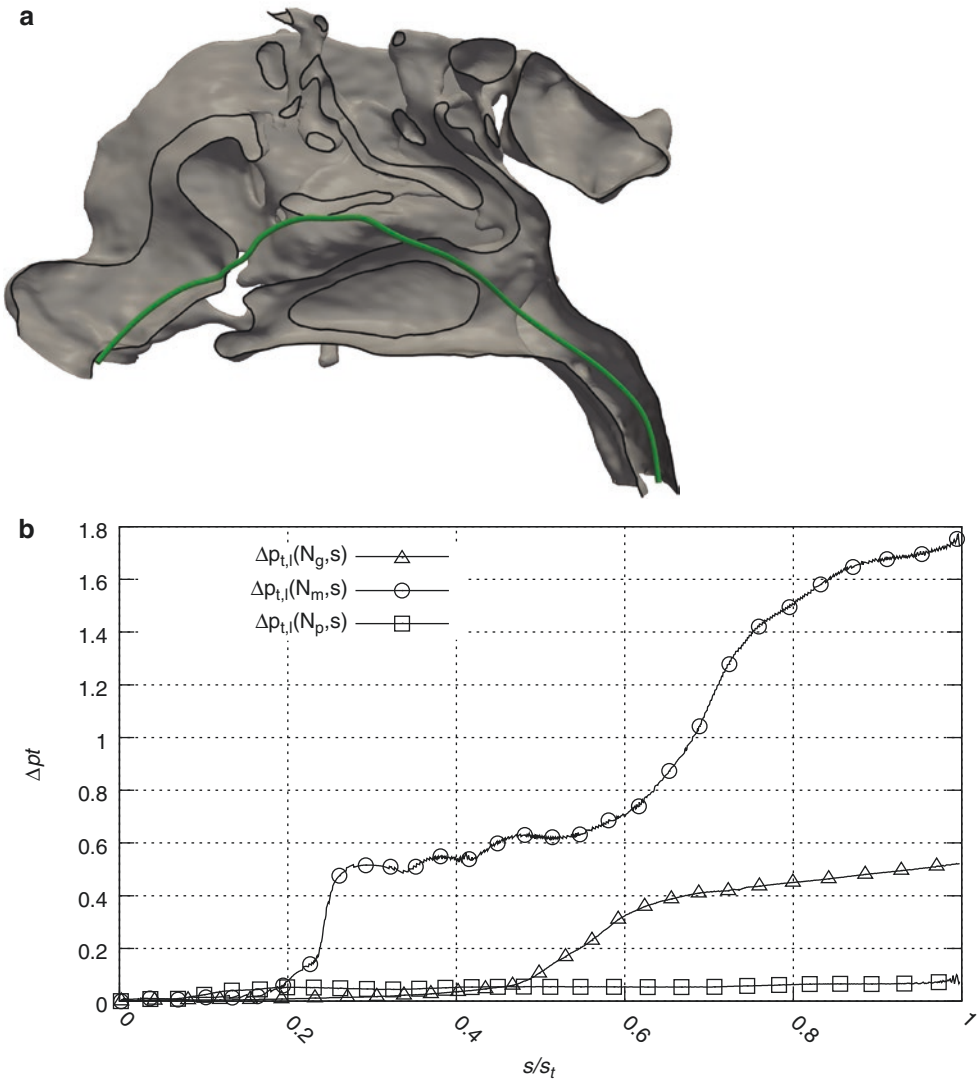

Fig. 9.2 Analysis of the total pressure loss along streamlines in three different nasal cavities on the left side (subscript *'l'*, patient view) as prformed in [15]. Note that Δp_t is in its non-dimensional form and that the arc length s has been normalized to 1 with the total arc length of the streamline st. (**a**) Surface of one of the nasal cavities and a streamline for which in (**b**) the according accumulated pressure loss is shown. (**b**) Accumulated total pressure loss along streamlines in three different nasal cavities. The plot for N_m corresponds to the cavity shown in (**a**)

Streamlines are not only a great tool to analyze the pressure loss, but can also be used to understand the distribution of the flow in the nasal cavity. That is, if they are colored, e.g., by the velocity magnitude of the flow, one can identify accelerating and decelerating flow [10, 11, 13, 15, 21] and hence positions of airway restrictions, i.e., locations that are potential regions for a surgery. Furthermore, streamlines deliver the possibility to analyze the mass flux distribution in the nasal cavity as they basically represent the fate of massless point-particles travelling through the nasal cavity. As such, they can be used to understand why patients have a diminished olfactory functionality, e.g., in cases where streamlines do not pass the olfactory organ at inspiration. Furthermore, they enable to identify where the flow penetrates the tissue, or in other words, where the flow impinges in the nasal cavity. Figure 9.3a shows an example of a streamline visualization. The flow distributes in all three turbinate regions and accelerates along the nasal cavity due to converging channels.

Penetration, however, can much better be analyzed by considering the wall-shear stress, which is the force acting on the tissue due to the passing flow. The wall-shear stress is computed by taking the derivative of the fluid velocity in wall-normal direction and multiplying it with the dynamic viscosity of the fluid. As such, in high Reynolds-number flows with smaller boundary layers the velocity gradient at the wall is much steeper than in cases where a fluid passes a wall slowly. The wall-shear stress can simply be mapped to the surface of the nasal cavity. An example of such a mapping is shown in Fig. 9.3b. An analysis of the wall-shear stress distribution helps to identify regions that suffer from impinging fluid and potentially from inflammations. In addition to such a qualitative analysis, the wall-shear stress can also be analyzed with respect to locally appearing maxima and by its surface-area averaged values. Especially, latter approach allows to juxtapose wall-shear stress behaviors of different nasal cavities. Corresponding wall-shear stress

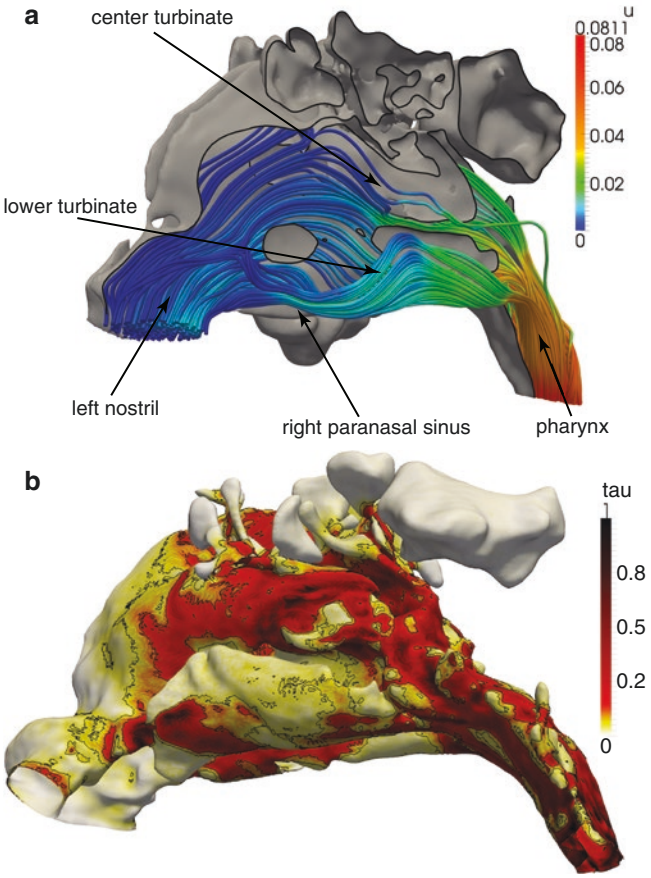

Fig. 9.3 Streamline and wall-shear stress visualizations taken from [15, 27]. (**a**) Streamlines in the nasal cavity colored by the non-dimensional velocity magnitude. (**b**) Non-dimensional wall-shear stress mapped to the tissue wall

computations for various nasal cavities have been performed in [4, 8, 12, 14, 15, 19, 35]. These investigations show that the wall-shear stress can be on the order of 1 *Pa* and that locally even higher stresses may occur, which may lead to inflammations inferred by the irritation of endothelial and epithelial cells. Furthermore, the evaluation of the wall-shear stress enables to identify local separation regions and small flux-diminishing channels, which could be potential candidates for a surgery.

The aforementioned evaluations did not consider the capability of the nasal cavity to temper the inhaled air. A healthy nasal cavity is, under the assumption of moderate ambient temperatures, capable of increasing the temperature up to almost body temperature before the fluid enters the lung. Hence, the temperature difference from the nostrils to the pharynx can be used to characterize the heating capability of a nasal cavity. Prescribing an ambient outside temperature at the nostrils and the body temperature at the tissue surface inside the nasal cavity allows to simulate the temperature distribution. An example of the temperature distribution in a nasal cavity can be found in Fig. 9.4a. It has to be mentioned that the inhalation of cold air also decreases the tissue temperature locally. To also model this effect, the heat transfer into the solid needs to be simulated as well. This, however, leads to a multi-physics problem, the necessity to model tissue properties, and new algorithmic challenges, i.e., finding coupling and parallelization strategies that efficiently solve such problems on HPC systems. Since the identifation of tissue properties is quite challenging and multi-physics implementations drastically increase code complexity, the simulation of the heat transfer is in general omitted although this may lead to loss of physical correctness. However, despite the fact that a fixed body temperature is assumed at the whole tissue wall, an approximate evaluation of the heating capability of a nasal cavity can be derived from the analysis of the temperature difference from nostrils to pharynx. Similar to the wall-shear stress computation, the heat flux into the fluid can be evaluated by the temperature gradient at the wall. If the flow passes close to the tissue, i.e., in the case of higher local Reynolds numbers, where the boundary layer is thin, the temperature gradient is strong and more heat is transferred into the fluid. In contrast, slow moving fluid and larger boundary layers lead to decreased heat fluxes. In the limit, when the fluid is at rest, the problem reduces to a simple heat diffusion problem as the convective part of the corresponding governing equation vanishes. Investigations of the heat flux and the temperature increase have been performed in [3, 14, 15]. The findings clearly show the capability of CFD simulations to analyze in detail where most of the heat is transported into the fluid. This is for example the case in the nasal valve or in the vicinity of the turbinates. Furthermore, in [15] a comparison of the thermal parameters for different nasal cavities revealed that those cavities that underwent a turbinectomy and hence having a smaller surface area to exchange heat with the fluid, suffer from a reduced heating capability.

As mentioned above, the Reynolds number defines the ratio of inertial forces to the viscous forces. It is a non-dimensional number that is commonly used in fluidmechanics to characterize the flow, i.e., if it is laminar, transitional, or turbulent. In nasal cavity flows the Reynolds number can, e.g., be defined by a reference velocity u that corresponds to a specific volume flux, the hydraulic diameter $D = 4 \cdot A/C$ with A being the area of the pharynx cross-section and C its circumference, and υ is the kinematic viscosity of air. As the velocity and the hydraulic diameter varies along the nasal cavity, it is obvious that the local Reynolds number Re_l also varies. In healthy nasal cavities, Re_l at peak inspiration at the pharynx is usually in the range of $Re_l \in (1000, 3000)$ and hence laminar to transitional, whereas in pathological cases the flow indeed may can become turbulent for locally larger Reynolds numbers [2, 5, 15, 16]. As such, strong fluctuating velocities emerge, which stem from small-scale vortical structures that are shed, e.g., from strong diameter variations

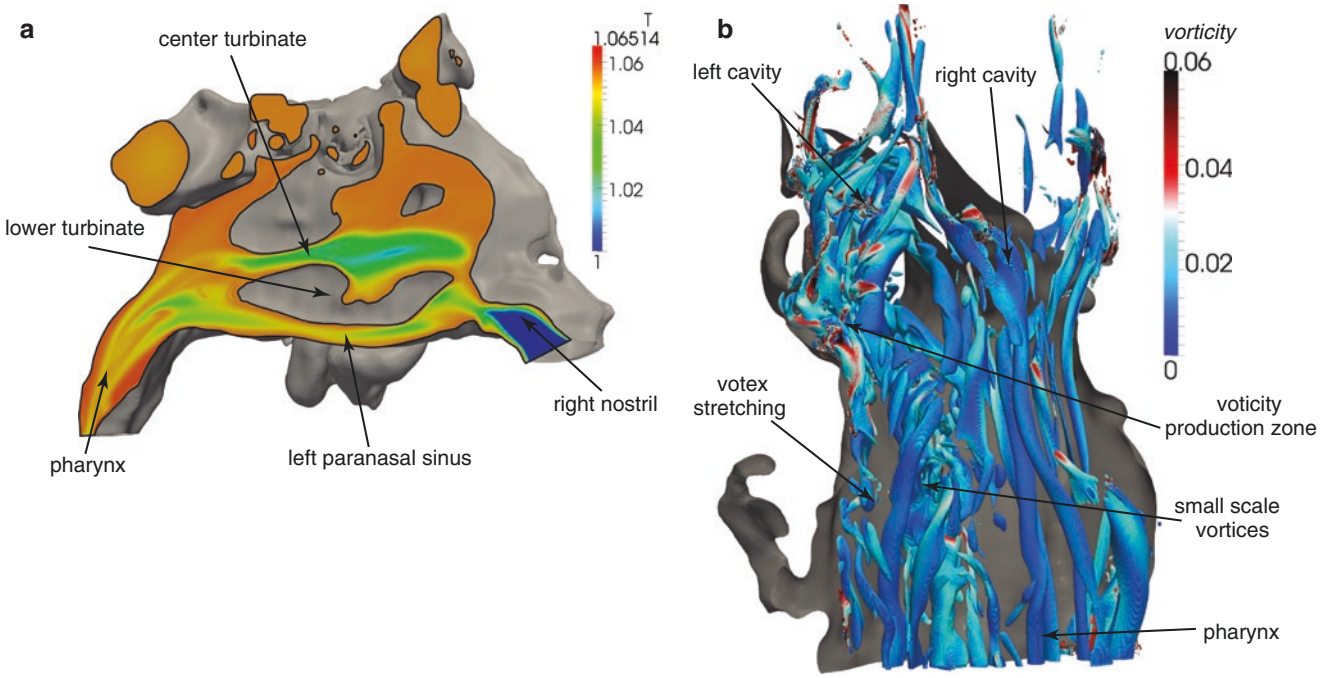

Fig. 9.4 Temperature distribution and visualization of transitional flow in the pharynx. Images were taken from [15, 27]. (**a**) Non-dimensional temperature distribution in the human nasal cavity. (**b**) Instantaneous transitional flow in the pharynx in a pathological nasal cavity. Vortices are detected by the Δ-criterion and the contours are colored by the vorticity

or sharp corners. Such phenomena increase the energy loss and hence contribute to the overall pressure loss of a nasal cavity. There exist several methods to analyze secondary flow structures like high-energetic vortices. Often such vortices are visualized by using some strain-rate-based vortex detection criteria, e.g., the λ_2-, Q-, or the Δ-criterion [37], to name just a few. Furthermore, the turbulent kinetic energy k that is derived from the Reynolds stresses can be used to identify high energetic regions in the flow field. An example of transitional flow in the pharynx region is depicted in Fig. 9.4b. For statistical analyses, the fluctuating flow is recorded over time at specified locations of interest. From the resulting time series, the frequency spectrum at such probe locations and correlations between different locations can be analyzed, i.e., information is gathered on the frequency of shed vortices and how information that is generated at one location is transported to another location. This helps to understand the fate of vortices, how they break up into smaller vortices, which way they are going, and if flow is turbulent or not. In [15, 16, 19], such in-depth analyses of the transitional or turbulent effects in respiration are investigated for the flow in the human nasal cavity, the larynx, and the trachea. In more detail, in [15, 19] energy spectra are used to show the mesh independence of the given solutions and to characterize the energy content of the flow at certain probe locations. Lintermann et al. [15] also present an analysis of eddy turnaround times by means of auto-correlations. They juxtapose cross-correlations to find correlating locations in the flow field and the turbulent kinetic energy is investigated similarly to [16]. CFD methods enable to investigate another essential functionality of the nasal cavity, namely its filtering function, i.e., the ability of catching particles that are dissolved in the fluid at inspiration. Examples of such particles are pollen, pollutants like fine dust particles or diesel aerosols, or even bacteria and other pathogens. For steady or time-averaged flow fields in which the according flow field does not change anymore, a particle simulation can be performed a posterior in a post-processing step of a flow computation. In contrast, highly unsteady flow fields require to track particles at CFD simulation run time. Frequently used approaches involve solving particle dynamics in addition to the governing equations of the flow. That is, in addition to an Eulerian ansatz for the flow, a Lagrangian ansatz for the particles is followed. In steady or averaged flow fields, the equation of motion for a particle uses the information of the non-changing flow field, which can be read from disk. In the unsteady case, an online-coupling for the solver of the fluid and the particle phase is necessary. It is obvious that the change of location of the particles also changes the workload per computational core, as they travel from one computational core to another. This leads to new parallelization issues that complicate implementations for efficient computation. Possible solutions either separate the solvers for flow and particle computation physically, which requires to communicate velocities across the according cores, or couple them directly on the core, where imbalance problems might appear [18]. Note

that such implementations mainly realize only a one-sided coupling, i.e., it is assumed that the particles are small, are transported by the motion of the fluid, and do not influence the flow. An analysis of the deposition behavior using particle simulation methods enables to evaluate the filtering function of the nasal cavity. Furthermore, this also allows for efficiency estimations of drug delivery under certain flow conditions, e.g., for respiration at rest or by considering sniffing processes. Several publications investigate particle-laden flow in the nasal cavity [6, 8, 17, 18, 20]. Shang et al. [17] analyze the influence of including facial features into the simulation and indeed find a difference in the deposition behavior to not including them. In contrast, in [6, 8, 18, 20], only the nasal cavity from the nostrils to the pharynx is considered and analyses are performed for different Reynolds numbers and particle sizes and particle/air density ratios. Particularly in [20], the focus is on drug delivery, i.e., on biopharamceuticals that are targeted at the olfactory cleft to treat brain pathologies. Basically, all investigations show that the nasal valve filters a certain amount of the particles and that small channels also increase the deposition behavior. However, this is strongly dependent on the Reynolds number, which varies for respiration at rest, under workout, or performing a sniff, the individual geometry, and the particle size and density ratio. It should be noted that in none of the aforementioned publications a tissue movement or the inclusion of nasal hair is included.

9.5 Potentials of Using CFD Methods in Clinical Applications

The methods described in Sect. 9.4 allow for patient-specific diagnoses and treatments, e.g., by supporting planning of surgical interventions or drug delivery disperses. Full DNS computations require to run simulations at present for several hours on tens of thousands of cores to solve a problem on meshes with a number of cells on the order of $O(10^9)$. Hence, an integration of such methods into clinical applications is currently not feasible and only make sense for research institutions that are interested in all detail of the flow physics. However, computing power becomes more and more inexpensive, which makes the use of LES more and more attractive. It should be noted that the continuous increase of computational power will also make the integration of DNS into clinical applications possible in the near future. It is expected that with the introduction of exascale HPC systems such simulations may be performed patient-specifically on demand. The integration of RANS computations is already possible nowadays but, as elaborated in Sect. 9.3, RANS should not be the method of choice due to its disadvantages for accurately predicting low-Reynolds number flows in complex geometries. Potentials that arise from the integration of CFD into the clinical work routine are

- Pre-surgical analyses of a nasal cavities from a fluid-mechanics point of view
  It is obvious that the methods described in Sect. 9.4 add to the understanding of the intricate flow in the human nasal cavity. They help to analyze why patients have problems in breathing by considering either the pressure loss along a streamline or the total area-averaged pressure loss along the whole nasal cavity. Streamlines allow for an analysis of the mass flux distribution, where most of the fluid is passing the nasal cavity, and if the air is guided past the olfactory organ. Wall-shear stress computations allow for an evaluation of the forces acting on the tissue and help to identify irritated regions that are potential candidates for a surgery. The heating capability and the heat flux distribution help to identify the origin of lung diseases, i.e., if a nasal cavity is able to heat up the air to body temperature. Statistical analyses and the visualization of vortex criteria furthermore add to the understanding if a flow is laminar, transitional, or turbulent. These methods enable to localize high energetic regions that produce secondary flow structures increasing the pressure loss.
  Planning a surgery hence would greatly benefit from such a detailed analysis that considers the geometry and the pathology of the individual patient. Creating diagnostic tools based on CFD computations requires, however, interdisciplinary cooperations between fluid-mechanics specialists, HPC and medical experts such that surgeons can optimally be supported.
- Analysis of the effectiveness of standardized surgery techniques
- The outcome of surgeries is often not known and surgeons rely on their experience when it comes, e.g., to the ablation or removal of tissue in the nasal cavity. CFD methods, however, may help to better understand the outcome of standardized surgery methods by performing pre- and post-surgical simulations. Hospital databases contain a large amount of medical image data sets, which hold information on the pathological state before a surgery and the post-surgical state. Using those images as a basis for an analysis of the change in pressure loss, the wall-shear stress distribution, and heating capability, it is possible to evaluate the method of surgery and to identify and predict successful procedures. Additionally, by using pre-surgical image data and the corresponding extracted surfaces in virtual operations, doctors can be trained to perform better surgeries as they get direct feedback from the results of CFD simulations. Future robotic systems could furthermore be tuned with respect to the CFD results to enhance surgery outcomes.

- Shape-optimization of nasal cavities
- Combining flow computations with shape optimization techniques is a natural extension of the existing methods. This way, surgeons will be able to define regions of the nasal cavity that they would consider for an operation. The three-dimensional surface representation extracted from medical images serves as a model that a virtual surgery could be performed on. The outcome of such a virtual surgery is a labeling that defines tissue segments to be removed and for which an optimal shape is a priori not known. Using then, in conjunction with CFD methods, shape optimization algorithms, e.g., adjoint-based methods, steepest-gradients, or implementations of sensitivity functions, it is possible to find optimal shapes that minimize or maximize certain objective functions. As such, the pressure loss or the wall-shear stress can be subject to minimization, while the heat flux or the heating capability should be maximized. The output is a surface that fulfills these constraints and which can be used as a template for a surgery. Note that such approaches have not been performed so far and that shape optimization for CFD is an expensive method and is still an active field of research.
- Drug-delivery optimization
- Using coupled flow and particle simulations, it is possible to track individual particles in an unsteady flow. This enables to optimize the delivery of drugs via the olfactory cleft to the human brain or to treat allergic rhinitis. Sprays are commonly used for such treatments, i.e., small vials with spray nozzles that break up the fluid into small ligaments and finally into separate droplets upon pumping. Obviously, the nozzle position and the type of respiration determine the fate of the drug. By numerical simulation, the optimal location, nozzle insertion angle, and respiration type for the individual application and even patient can be determined to maximize the effectiveness of the drug.
- Enhancement of rhinological diagnoses with the help of machine learning techniques
  The collection of all available patient data, i.e., image data, diagnostic data such as anamese reports, rhinomanometer measurements, and historical reports in combination with simulation results enable the use of machine learning measurements, and historical reports in combination with simulation results enable the use of machine learning techniques to support surgical diagnoses. That is, segmentation of CT data could be performed fully automatically with the help of articifical neural networks, pathologies could be classified automatically, flow physics could be predicted by means of physics-based learning methods circumventing expensive CFD computations, and pathological features could be extracted automatically and presented to the medical doctor for further consideration.

References

1. Naftali S, Schroter RC, Shiner RJ, Elad D. Transport phenomena in the human nasal cavity: a computational model. Ann Biomed Eng. 1998;26(5):831–9.
2. Hörschler I, Meinke M, Schröder W. Numerical simulation of the flow field in a model of the nasal cavity. Comput Fluids. 2003; 32(1):39–45. https://doi.org/10.1016/S0045-7930(01)00097-4.
3. Naftali S, Rosenfeld M, Wolf M, Elad D. The air-conditioning capacity of the human nose. Ann Biomed Eng. 2005;33(4):545–53. https://doi.org/10.1007/s10439-005-2513-4.
4. Elad D, Naftali S, Rosenfeld M, Wolf M. Physical stresses at the air-wall interface of the human nasal cavity during breathing. J Appl Physiol. 2006;100(3):1003–10. https://doi.org/10.1152/japplphysiol.01049.2005.
5. Hörschler I, Schröder W, Meinke M. On the assumption of steadiness of nasal cavity flow. J Biomech. 2010;43(6):1081–5. https://doi.org/10.1016/j.jbiomech.2009.12.008.
6. Shi H, Kleinstreuer C, Zhang Z. Dilute suspension flow with nanoparticle deposition in a representative nasal airway model. Phys Fluids. 2008;20(1):013301. https://doi.org/10.1063/1.2833468.
7. Zachow S, Muigg P, Hildebrandt T, Doleisch H, Hege HC. Visual exploration of nasal airflow. IEEE Trans Vis Comput Graph. 2009;15(6):1407–14. https://doi.org/10.1109/TVCG.2009.198.
8. Gambaruto A, Taylor D, Doorly D. Modelling nasal airflow using a Fourier descriptor representation of geometry. Int J Numer Methods Fluids. 2009;59(11):1259–83. https://doi.org/10.1002/fld.1866.
9. Riazuddin VN, Zubair M, Shuaib IL, Abdullah MZ, Hamid SA, Ahmad KA. Numerical study of inspiratory and expiratory flow in a human nasal cavity. J Med Biol Eng. 2010;31(3):201–6. https://doi.org/10.5405/jmbe.781.
10. Lintermann A, Meinke M, Schröder W. Investigations of nasal cavity flows based on a lattice- Boltzmann method, in: Resch M, Wang X, Bez W, Focht E, Kobayashi H, Roller S (Eds.), High performance computing on vector systems 2011, Springer Berlin, 2012, pp. 143–158. doi:https://doi.org/10.1007/978-3-642-22244-3.
11. Lintermann A, Meinke M, Schröder W. Investigations of the Inspiration and Heating Capability of the Human Nasal Cavity Based on a Lattice-Boltzmann Method. In: Proceedings of the ECCOMAS Thematic International Conference on Simulation and Modeling of Biological Flows (SIMBIO 2011), Brussels, Belgium, 2011.
12. Gambaruto AM, Taylor DJ, Doorly DJ. Decomposition and description of the nasal cavity form. Ann Biomed Eng. 2012;40(5):1142–59. https://doi.org/10.1007/s10439-011-0485-0.
13. Achilles N, Pasch N, Lintermann A, Schröder W, Mösges R. Computational fluid dynamics: a suitable assessment tool for demonstrating the antiobstructive effect of drugs in the therapy of allergic rhinitis. ActaotorhinolaryngologicaItalica: organoufficialedella Societ'aitaliana di otorinolaringologia e chirurgiacervico-facciale. 2013;33(1):36–42.
14. Kim SK, Na Y, Kim JI, Chung SK. Patient specific CFD models of nasal airflow: overview of methods and challenges. J Biomech. 2013;46(2):299–306. https://doi.org/10.1016/j.jbiomech.2012.11.022.
15. Lintermann A, Meinke M, Schröder W. Fluid mechanics based classification of the respiratory efficiency of several nasal cavities. Comput Biol Med. 2013;43(11):1833–52. https://doi.org/10.1016/j.compbiomed.2013.09.003.
16. Bates AJ, Doorly DJ, Cetto R, Calmet H, Gambaruto AM, Tolley NS, et al. Dynamics of airflow in a short inhalation. J R Soc Interface. 2014;12(102):20140880. https://doi.org/10.1098/rsif.2014.0880.
17. Shang Y, Inthavong K, Tu J. Detailed micro-particle deposition patterns in the human nasal cavity influenced by the breathing zone. Comput Fluids. 2015;114:141–50. https://doi.org/10.1016/j.compfluid.2015.02.020.

18. Henn T, Thäter G, Dörfler W, Nirschl H, Krause MJ. Parallel dilute particulate flow simulations in the human nasal cavity. Comput Fluids. 2016;124:197–207. https://doi.org/10.1016/j.compfluid.2015.08.002.
19. Calmet H, Gambaruto A, AM BAJ, Vázquez M, Houzeaux G, Doorly DJ. Large-scale CFD simulations of the transitional and turbulent regime for the large human airways during rapid inhalation. Comput Biol Med. 2016;69:166–80. https://doi.org/10.1016/j.compbiomed.2015.12.003.
20. Engelhardt L, Röhm M, Mavoungou C, Schindowski K, Schafmeister A, Simon U. First steps to develop and validate a CFPD model in order to support the Design of Nose-to-Brain Delivered Biopharmaceuticals. Pharm Res. 33:1337. https://doi.org/10.1007/s11095-016-1875-7.
21. Eitel G, Freitas RK, Lintermann A, Meinke M, Schröder W. Numerical simulation of nasal cavity flow based on a lattice-Boltzmann method. In: Dillmann A, Heller G, Klaas M, Kreplin HP, Nitsche W, Schröder W, editors. New results in numerical and experimental fluid mechanics VII, 112 of notes on numerical fluid mechanics and multidisciplinary design. Berlin: Springer; 2010. p. 513–20.
22. Lorensen WE, Cline HE. Marching cubes: a high resolution 3D surface construction algorithm. ACM SIGGRAPH Computer Graphics. 1987;21(4):163–9.
23. Taubin G, Zhang T, Golub G. Optimal surface smoothing as filter design. Computer Vision ECCV. 1996;96:283–92.
24. Fedorov A, Beichel R, Kalpathy-Cramer J, Finet F-RJJC, Pujol S, et al. 3D slicer as an image computing platform for the quantitative imaging network. Magn Reson Imaging. 2012;30(9):1323–41. https://doi.org/10.1016/j.mri.2012.05.001.
25. Nolden M, Zelzer S, Seitel A, Wald D, Müller M, Franz AM, et al. The medical imaging interaction toolkit: challenges and advances. Int J Comput Assist Radiol Surg. 2013;8(4):607–20. https://doi.org/10.1007/s11548-013-0840-8.
26. Rosset A, Spadola L, Ratib O. Osiri X. an open-source software for navigating in multidimensional DICOM images. J Digit Imaging. 2004;17(3):205–16. https://doi.org/10.1007/s10278-004-1014-6.
27. Lintermann A, Schlimpert S, Grimmen J, Günther C, Meinke M, Schröder W. Massively parallel grid generation on HPC systems. Comput Methods Appl Mech Eng. 2014;277:131–53. https://doi.org/10.1016/j.cma.2014.04.009.
28. Chien KY. Predictions of channel and boundary-layer flows with a low-Reynolds-number turbulence model. AIAA J. 1982;20(1):33–8. https://doi.org/10.2514/3.51043.
29. Wilcox DC. Formulation of the k-omega turbulence model revisited, in: 45th AIAA aerospace sciences meeting and exhibit, American Institute of Aeronautics and Astronautics, Reston, Virigina, 2007. doi:10.2514/6.2007-1408.
30. Anderson JDJ. Computational fluid dynamics. Singapore: MacGraw-Hill; 1995.
31. Succi S. The lattice Boltzmann equation: theory and applications, vol. 222. Rome: Oxford University Press; 2001.
32. Kopriva DA. Implementing spectral methods for partial differential equations, scientific computation. Dordrecht: Springer. https://doi.org/10.1007/978-90-481-2261-5.
33. Bernoulli D. Hydrodynamica, sive de viribus et motibusfluidorumcommentarii: opus academicumabauctore, dumPetropoliageret, congestum, 1738. doi:https://doi.org/10.3931/e-rara-3911.
34. Finck M, Hänel D, Wlokas I. Simulation of nasal flow by lattice Boltzmann methods. Comput Biol Med. 2007;37(6):739–49. https://doi.org/10.1016/j.compbiomed.2006.06.013.
35. Hörschler I, Schröder W, Meinke M. Comparison of steady and unsteady nasal cavity flow solutions for the complete respiration cycle. Comput Fluid Dyn J. 2006;15(3):354–77.
36. Vogt K, Hoffrichter H. Neuesträmungs physikalische Erkenntnisse in der Rhinomanometrie und ihrepraktischenKonsequenzen. In: Mösges S, editor. TopischeTherapie der allergischen Rhinitis. Germany: Biermann; 1993. p. 45–60.
37. Haller G. An objective definition of a vortex. J Fluid Mech. 2005;525:1–26. https://doi.org/10.1017/S0022112004002526.